Royal College of Surgeons in Ireland

repository@rcsi.com

Growth plate extracellular matrix-derived scaffolds for large bone defect healing.

AUTHOR(S)

G M. Cunniffe, P J. Díaz-Payno, J S. Ramey, O R. Mahon, A Dunne, Emmet M. Thompson, Fergal O'Brien, Daniel J. Kelly

CITATION

Cunniffe, G M.; Díaz-Payno, P J.; Ramey, J S.; Mahon, O R.; Dunne, A; Thompson, Emmet M.; et al. (2017): Growth plate extracellular matrix-derived scaffolds for large bone defect healing.. Royal College of Surgeons in Ireland. Journal contribution. https://hdl.handle.net/10779/rcsi.10767011.v2

HANDLE

10779/rcsi.10767011.v2

LICENCE

CC BY-NC-SA 4.0

This work is made available under the above open licence by RCSI and has been printed from https://repository.rcsi.com. For more information please contact repository@rcsi.com

URL

https://repository.rcsi.com/articles/journal_contribution/Growth_plate_extracellular_matrix-derived_scaffolds_for_large_bone_defect_healing_/10767011/2

European Cells and Materials Vol. 33 2017 (pages 130-142) DOI: 10.22203/eCM.v033a10 ISSN 1473-2262

GROWTH PLATE EXTRACELLULAR MATRIX-DERIVED SCAFFOLDS FOR LARGE BONE DEFECT HEALING

G.M. Cunniffe[1,2,3], P.J. Díaz-Payno[1,2,3], J.S. Ramey[1], O.R. Mahon[4], A. Dunne[4], E.M. Thompson[3,5], F.J. O'Brien[1,2,3,5] and D.J. Kelly[1,2,3,5]*

[1] Trinity Centre for Bioengineering, Trinity Biomedical Sciences Institute, Trinity College Dublin, Dublin, Ireland.
[2] Department of Mechanical and Manufacturing Engineering, School of Engineering, Trinity College Dublin, Dublin, Ireland.
[3] Advanced Materials and Bioengineering Research Centre (AMBER), Royal College of Surgeons in Ireland and Trinity College Dublin, Dublin, Ireland.
[4] Molecular Immunology Group, School of Biochemistry and Immunology, Trinity College Dublin, Dublin, Ireland.
[5] Tissue Engineering Research Group, Department of Anatomy, Royal College of Surgeons in Ireland, 123 St. Stephen's Green, Dublin 2, Ireland

Abstract

Limitations associated with demineralised bone matrix and other grafting materials have motivated the development of alternative strategies to enhance the repair of large bone defects. The growth plate (GP) of developing limbs contain a plethora of growth factors and matrix cues which contribute to long bone growth, suggesting that biomaterials derived from its extracellular matrix (ECM) may be uniquely suited to promoting bone regeneration. The goal of this study was to generate porous scaffolds from decellularised GP ECM and to evaluate their ability to enhance host mediated bone regeneration following their implantation into critically-sized rat cranial defects. The scaffolds were first assessed by culturing with primary human macrophages, which demonstrated that decellularisation resulted in reduced IL-1β and IL-8 production. *In vitro*, GP derived scaffolds were found capable of supporting osteogenesis of mesenchymal stem cells *via* either an intramembranous or an endochondral pathway, demonstrating the intrinsic osteoinductivity of the biomaterial. Furthermore, upon implantation into cranial defects, GP derived scaffolds were observed to accelerate vessel in-growth, mineralisation and *de novo* bone formation. These results support the use of decellularised GP ECM as a scaffold for large bone defect regeneration.

Keywords: Growth plate, Extracellular matrix, Scaffold, Large bone defect regeneration, Scaffold immune response.

*Address for correspondence:
Prof. Daniel Kelly
Trinity Centre for Bioengineering,
Trinity Biomedical Sciences Institute,
152-160 Pearse Street, Dublin 2, Ireland
Telephone: +353-1-8963947
E-mail: kellyd9@tcd.ie

Introduction

The repair of large bone defects still presents a significant clinical challenge, with the use of autografting material remaining the gold standard treatment despite the drawbacks associated with this approach (Dimitriou *et al.*, 2011). Biological scaffolds derived from animal and human extracellular matrix (ECM), which are composed of instructive structural and functional molecules to facilitate tissue regeneration, have been successfully used clinically to repair numerous different tissues and organs (Benders *et al.*, 2013). Demineralised bone matrix is commonly used in bone regeneration (Gruskin *et al.*, 2012; Solheim, 1998), although concerns remain as to its osteoinductivity (Aghdasi *et al.*, 2013; An *et al.*, 1995; Tilkeridis *et al.*, 2014). Long bones form by the coordinated process of endochondral ossification, with the postnatal growth and development of our limbs driven by the growth plates (also called the epiphyseal plates). The growth plate (GP) is known to contain members of the transforming growth factor (TGF)-β family, including bone morphogenetic protein (BMP), as well as vascular endothelial growth factor (VEGF) and Indian hedgehog (Ihh), which are known to be strongly osteoinductive (Alini *et al.*, 1992; Anderson *et al.*, 2000; Carlevaro *et al.*, 2000; Gerber *et al.*, 1999; Kronenberg, 2003; Nilsson *et al.*, 2007; Qiu *et al.*, 2015; Wang *et al.*, 2004). Indeed, powdered demineralised GP has been shown to be osteoinductive *in vivo*, supporting the development of a bone ossicle following ectopic implantation into rats (Bigham *et al.*, 2011). Clearly, such ECM derived biomaterials have tremendous potential for bone regeneration; however, realising this potential requires processing them into biological scaffolds capable of facilitating vascularisation and host osteo-progenitor mediated bone formation.

The ideal scaffold for bone regeneration is biocompatible, allows for cell infiltration and provides instructive cues to infiltrating cells, preferably to induce an osteogenic response. Porous scaffolds produced using collagen and hydroxyapatite, the two main constituents of bone, have been shown to encourage osteogenesis of MSCs *in vitro* and can support bone regeneration *in vivo* (Calabrese *et al.*, 2016; Chen *et al.*, 2015; Cunniffe *et al.*, 2010; Cunniffe and O'Brien, 2011; David *et al.*, 2015; Gleeson *et al.*,

2010; Prosecka *et al.*, 2015; Villa *et al.*, 2015). Ideally scaffolds have an open interconnected pore structure, with pore sizes in the range of 85-325 μm best supporting osteogenesis (Karageorgiou and Kaplan, 2005; Murphy *et al.*, 2010; O'Brien *et al.*, 2007). The osteoinductivity of these scaffolds can be improved by the incorporation of gene and growth factors such as BMP-2 and VEGF (Quinlan *et al.*, 2015a; Quinlan *et al.*, 2015b; Samorezov and Alsberg, 2015), although it remains uncertain as to what is the ideal combination of matrix components and growth factors to safely induce osteogenesis without the need for excessive levels of growth factors.

Rather than building a bone mimetic scaffold from the bottom-up using collagen and mineral components found in bone, and then systematically incorporating growth factors into such a construct, the goal of this study was instead to produce a porous osteoinductive scaffold from decellularised growth plate, the precursor matrix of long bones. Native and *in vitro* cell culture derived ECMs are commonly used to produce scaffolds for tissue engineering (Almeida *et al.*, 2014; Cunniffe *et al.*, 2015; Jin *et al.*, 2007; Kheir *et al.*, 2011; Kim *et al.*, 2015; Lau *et al.*, 2012; Lu *et al.*, 2011; Pati *et al.*, 2015; Pattabhi *et al.*, 2014; Sutherland *et al.*, 2015); however, the ideal matrix to facilitate bone regeneration has yet to be established. As previously stated, the GP matrix contains many important growth factors for inducing bone growth which render it as an attractive option for generating an osteoinductive ECM derived scaffold. The hypothesis of this study is that a decellularised GP ECM derived scaffold will support vascularisation and accelerated bone formation following implantation into critically-sized defects. The first objective of the study was to decellularise GP ECM and to use this biomaterial to produce a porous scaffold. We next evaluated the osteoinductivity of this scaffold *in vitro* by assessing its capacity to promote osteogenesis of MSCs *via* either an intramembranous or an endochondral pathway. The final phase of the study assessed the capacity of these scaffolds to support healing of critically-sized rat cranial defects.

Materials and Methods

Decellularisation and scaffold fabrication

Growth plate (GP) tissue was harvested from the femur and tibia of porcine hind limbs (3-4 months old) shortly after sacrifice. The GP region was reached by sawing the bone through the long axis, and breaking the bone open along the softer GP region, allowing the GP tissue to be scraped out in small pieces using a scalpel (~1 mm^3). These small pieces were then minced in distilled H_20 using a homogeniser (IKAT10, IKA® Works Inc., NC, USA) to create an ECM slurry. The effect of decellularisation was evaluated, comparing native GP (no additional treatment prior to freeze-drying), to a detergent-based technique using 0.1 % sodium dodecyl sulphate (SDS; Sigma-Aldrich); following comparisons with other detergents commonly used for decellularisation (Cheng *et al.*, 2014; Gilbert *et al.*, 2006; Luo *et al.*, 2016; Luo *et al.*, 2015), results not shown. Decellularised GP slurry underwent two freeze-thaw cycles in a hypotonic buffer (10 mM Trizma hydrochloride and 5 mM ethylenediaminetetraacetic acid (EDTA) at pH 7.4), washed in saline (PBS), and treated for 1 h at room temperature in 0.1 % SDS. Following subsequent PBS washes, the slurry was placed in a DNase/RNase solution (5 mM $MgCl_2$, 10 U/mL of DNase, and 10 U/mL of RNase) and incubated for 1 h at 37 °C. Following this initial evaluation, all succeeding GP scaffolds used in the *in vitro* and *in vivo* studies were decellularised using this method.

The homogenised tissues (native GP, or decellularised GP) were centrifuged and the supernatant was removed. The remaining material was re-suspended in distilled H_2O at a concentration of 500 mg/mL. The slurry was transferred to custom-made specific polydimethylsiloxane (PDMS) cylindrical moulds (resulting in constructs of 5 mm × 3 mm for *in vitro,* and 7 mm × 2 mm for *in vivo* studies) and freeze-dried (Triad, Labconco, KC, USA) to produce porous scaffolds. Briefly, the slurry temperature was reduced to −30 °C (1 °C/min) and maintained for 1 h to allow for ice-crystal nucleation and growth. The temperature was then increased to −10 °C (1 °C/min), followed by a hold of 24 h to allow for sublimation of the liquid phase, and then finally increased to room temperature (0.5 °C/min). Scaffolds then underwent dehydrothermal crosslinking (DHT) as previously described in the literature (Haugh *et al.*, 2009). The DHT process was performed in a vacuum oven (VD23, Binder, Germany), at 105 °C, at 0.5 mbar for 24 h. This was then followed by a chemical cross-linking treatment using 1-Ethyl-3-(3-dimethylaminopropyl) carbodiimide (EDAC; 6 mM for 2 h with two washes in sterile phosphate buffered saline 2 × 1 h). Scaffolds were either seeded with cells for the *in vitro* analysis, or implanted cell-free for the *in vivo* study.

Scanning Electron Microscopy (SEM)

Scaffolds were imaged using SEM to visualise the internal porous structure of the freeze-dried constructs. Imaging was carried out following DHT treatment by fixing constructs to an adhesive carbon stub, sputter coating with gold, and imaging using a lens detector with a 5 kV acceleration voltage at calibrated magnifications (Tescan Mira XMU, Tescan USA Inc.).

Biochemical analysis of DNA, sGAG and calcium

Scaffolds formed from native GP, and decellularised GP matrix were evaluated (n = 3) for their residual DNA, sulphated glycosaminoglycan (sGAG) and calcium content post fabrication. Scaffolds were digested with papain (125 μg mL^{-1}) in 0.1 M sodium acetate, 5 mM L-cysteine-HCl, 0.05 M EDTA, pH 6.0 (all from Sigma-Aldrich) at 60 °C and 10 rpm for 18 h. DNA content was quantified using the Hoechst Bisbenzimide 33258 dye assay, with a calf thymus DNA standard (Sigma-Aldrich). The amount of sGAG was quantified using the dimethyl methylene blue (DMMB) dye-binding assay (Blyscan, Biocolor Ltd., Northern Ireland), with a chondroitin sulphate standard and both were normalised by scaffold weight. To quantify calcium deposition, scaffolds were chemically digested in 1 M HCL at 60 °C under rotation for 18 h, and an O-cresolphthalein complexone (oCPC; Sentinel Diagnostics, Italy) assay was performed. Cell-seeded

constructs were also analysed (n = 3) for their sGAG and calcium content following 28 d in culture using the same protocols.

Innate immune response analysis

Cytokine production measured by ELISA

In order to characterise the immune cell response to the native and decellularised GP scaffolds, primary human macrophages were seeded onto the scaffolds and analysed. Peripheral blood mononuclear cells (PBMC) were isolated by means of density gradient centrifugation from leukocyte-enriched buffy coats from anonymous healthy donors, obtained with permission from the Irish Blood Transfusion Board, St. James's Hospital, Dublin. CD14+ myeloid cells were purified from PBMC by means of positive selection using anti-CD14 magnetic beads according to the manufacturer's protocol (Miltenyi Biotech, Germany) (Corr *et al.*, 2016; Safi *et al.*, 2016). Cells were shown to be >90 % pure as determined by flow cytometry. $CD14^+$ monocytes were differentiated into macrophages for 6 d in the presence and absence growth plate scaffolds using M-CSF (50 ng/mL). As a positive control, macrophages were also stimulated with 100 ng/mL LPS for 24 h. Cytokine production was quantified in cell supernatants by ELISA (IL-1β and TNF, R&D Systems; IL-12 and IL-8, eBiosciences).

Real-time PCR

Primary human macrophages ($7.5 \times 10^{\wedge 5}$ cells/mL) were polarised to an M1 phenotype with IFNγ (10 ng/mL) for 24 h in the presence and absence of native and decellularised GP scaffolds. RNA was extracted from cells using the High Pure RNA Isolation Kit (Roche, Basel, Switzerland) and assessed for concentration and purity using the NanoDrop 2000c UV-Vis spectrophotometer. RNA was equalised and reverse transcribed using the Applied Biosystems High-Capacity cDNA reverse transcription kit. Real-time quantitative PCR was carried out on triplicate cDNA samples with the use of the CFX96 Touch Real-Time PCR Detection System (Bio-Rad Laboratories, Hercules, California). Real-time PCR for the detection of CCL19 and CXCL11 mRNA was performed using the TaqMan fast universal PCR Master Mix (Applied Biosystems) and predesigned TaqMan gene expression primers. Amounts of mRNA were normalised relative to the housekeeping gene Ribosomal Protein 18S.

In vitro analysis with bone marrow derived MSCs

Bone marrow derived mesenchymal stem cells (BMSCs) were harvested from the femora of porcine hind legs, and expanded using standard culture conditions. BMSCs were expanded to passage 2 and seeded onto the GP scaffold at a density of $0.5 \times 10^{\wedge 6}$ cells per scaffold. Cells were allowed to attach to the scaffolds for 1 h in the incubator at 37 °C before culturing in either chondrogenic or osteogenic medium for 28 d in normoxic conditions (20 % O_2 and 5 % CO_2). The constructs were cultured in 5 mL of either (i) chondrogenic media: Dulbecco's modified Eagle's medium (DMEM) + GlutaMAX™ (Gibco), 1 mM sodium pyruvate, 350 μM L-proline, 1.5 mg/mL bovine serum albumin (BSA), 1 nM dexamethasone, 300 μM ascorbic acid, 17 μM linolenic acid, 10 ng/mL transforming growth factor β3 (TGF-β3, ProSpec-Tany, Israel), 1X insulin-transferrin-selenium; or (ii) osteogenic media: DMEM + GlutaMAX™, 10 % foetal bovine serum (Gibco), 10 mM β-glycerophosphate, 1 nM dexamethasone, 0.09 mM ascorbic acid. Both media were supplemented with 100 units/mL penicillin, 100 units/mL streptomycin and 0.25 μg/mL amphotericin B.

Histology and immunohistochemistry

Samples were fixed in 4 % paraformaldehyde (PFA) overnight, dehydrated in a graded series of ethanol and xylenes, and embedded in paraffin wax. *In vivo* samples were decalcified following fixation using an EDTA treatment (15 % EDTA at pH 7.4) to remove the mineral component prior to embedding. Sections of 8 μm were obtained with a microtome (Leica RM2125RT) and affixed to microscope slides. Prior to staining, sections were dewaxed and rehydrated in 100-70 % ethanol followed by distilled water. The deposition of sGAG, collagen and calcium over 28 d *in vitro* was evaluated using 1 % alcian blue in 0.1 M HCl, picrosirius red, and 1 % alizarin red solutions respectively. Post-implantation samples were evaluated for cellular infiltration and bone matrix deposition with haematoxylin and eosin (H&E) and deposition of sGAG with safranin-O (all Sigma-Aldrich). Evaluation of vessel number and bone area quantification were performed on histological samples stained for H&E, by counting vessels visible across an entire section, under a microscope at 20×, and using Adobe Photoshop and Image J to determine bone area.

Collagen type II and type X deposition was evaluated using a standard immunohistochemical technique (Sheehy *et al.*, 2015). Briefly, sections (n = 4 sections per group) were treated with hydrogen peroxidase (Sigma-Aldrich), followed by enzymatic treatment with pronase (0.5 mg/mL, Merck Millipore) in a humidified environment for 5 min at 37 °C to enhance the permeability of the ECM. Sections were incubated with goat serum to block non-specific sites and mouse monoclonal IgG anti-collagen type II (ab3092, 1:100) and mouse monoclonal IgM anti-collagen type X (ab49945, 1:200) primary antibodies (Abcam) were applied overnight at 4 °C. Next, the secondary antibody (Collagen type II; goat anti-mouse IgG, 1:200, B7151 Sigma-Aldrich and Collagen type X; goat anti-mouse IgM, 1:200, ab49760 Abcam, UK) was added for 1 h, followed by incubation with ABC reagent (Vectastain PK-400, Vector Labs) for 45 min. Finally, sections were developed with DAB peroxidase (Vector Labs) for 5 min. Positive and negative controls were included in the immunohistochemistry staining protocol for each batch.

Cranial defect implantation

A cranial defect was created in adult male Fischer rats following an established procedure (Lyons *et al.*, 2010), with n = 4 animals per group at two time points of 4 and 8 weeks. Anaesthesia was induced with an intraperitoneal injection of xylazine hydrochloride (10 mg/kg) and ketamine hydrochloride (75 mg/kg), and maintained with inhalational isoflurane and oxygen (0.5-2 % isoflurane). A 7 mm circular transosseous defect was created on the

left side of the rat parietal calvarium using a grinding burr and the GP scaffold (decellularised but not EDTA-treated) was immediately implanted into the defect or left untreated for the empty defect (ED) groups before closing of the wound with sutures. Atipamezole hydrochloride was given to reverse sedation. Pain relief was administered *via* carprofen and buprenorphine subcutaneous injections over the following 2 d. On dates of scheduled explant retrieval, rats were sacrificed by CO_2 asphyxiation and cervical dislocation, and calvaria were harvested for evaluation. Ethical approval was given by the Research Ethics Committee of the Royal College of Surgeons in Ireland and an animal licence was granted by the Department of Health and Children (Ref. B100/4490) prior to initiation of study.

Micro-computed tomography

Micro-computed tomography (μCT) scans were carried out on the explants from the cranial study in order to visualise and quantify mineral content and distribution. A Scanco Medical 40 μCT system (Scanco Medical, Bassersdorf, Switzerland) was used for evaluation with a 70 kVp X-ray source at 114 μA. Four constructs were analysed per experimental group and per time point. Reconstructed 3D images were generated from the scans and used to visualise mineral distribution throughout the implanted scaffold or control group. Quantification was performed by setting a threshold of 165, corresponding to 339 mg HA/cm^3, and recording the bone volume (BV) within the defect per total volume (BV/TV), using a consistent total volume (5 mm diameter and 50 slices in the Z direction, voxel size 20 μm) from sample to sample which eliminated original bone from the calculations (Cunniffe *et al.*, 2016).

Statistical Analysis

All statistical analyses were carried out using GraphPad. The results are reported as means ± standard deviation. Groups were analysed by a general linear model for analysis of variance with groups of factors. Tukey's test or student *t*-tests were used to compare groups. Significance was accepted at a level of $p < 0.05$.

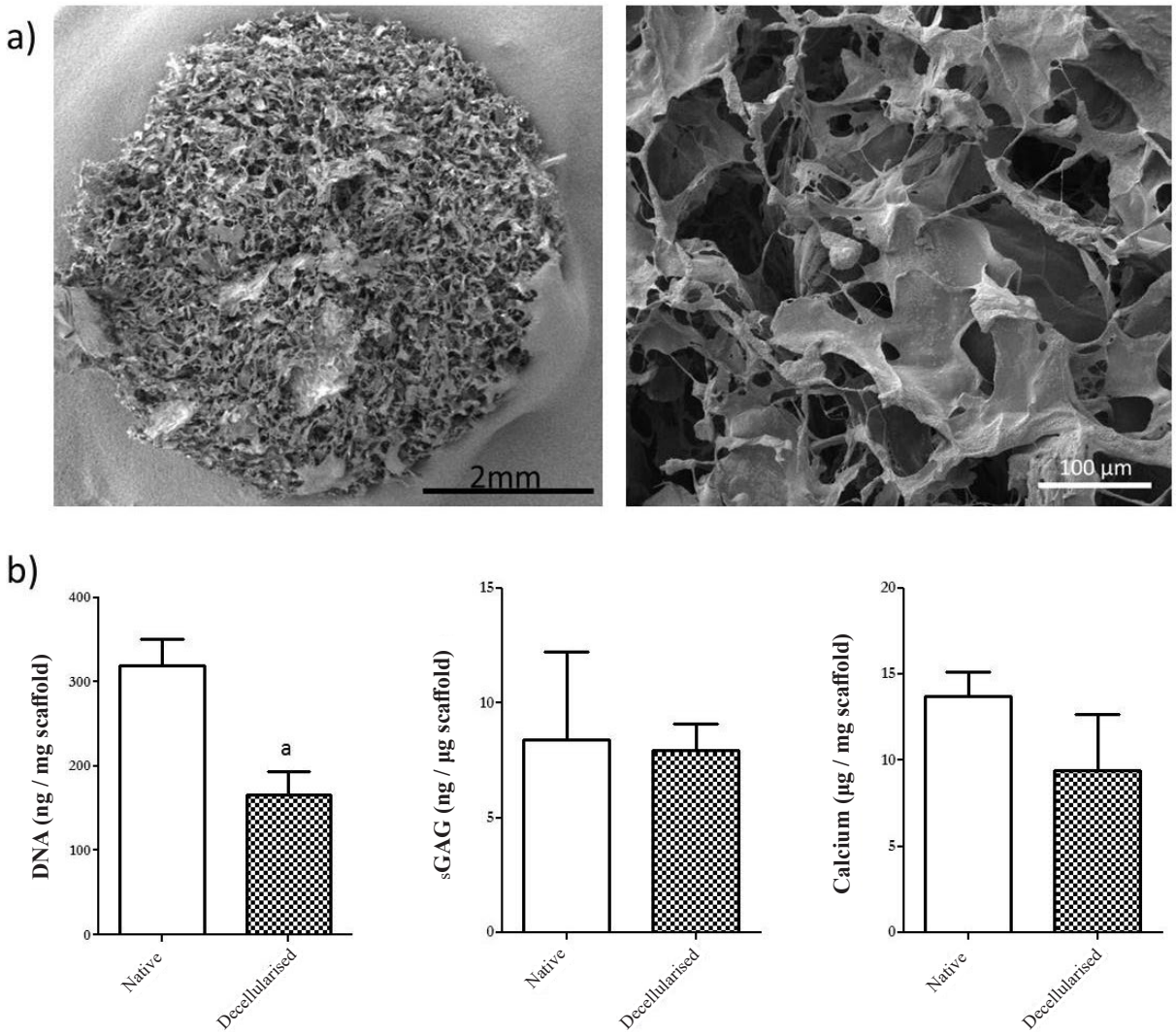


Fig. 1. **a**). Scanning electron microscopy (SEM) images of the GP scaffold indicating the open interconnected porosity achieved post-lyophilisation. **b**). Biochemical analysis of residual DNA, sGAG and calcium following the 0.1 % SDS decellularisation treatment, compared to the native GP scaffold. (**a**) $p<0.05$ (unpaired *t*-test).

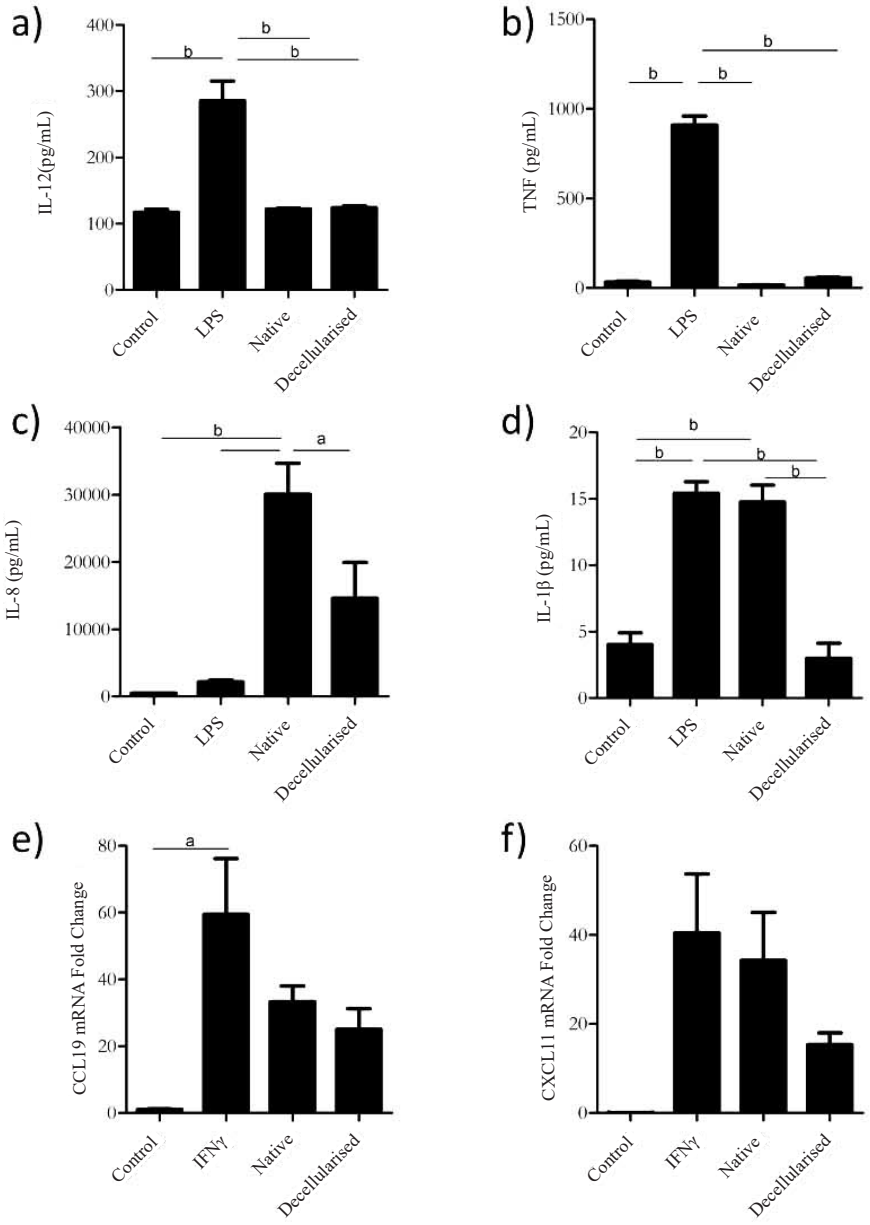


Fig. 2. **a**-**d**). The effect of growth plate scaffolds on cytokine production and macrophage phenotype. Human monocytes were differentiated into macrophages in the presence of native and 0.1 % SDS treated growth plate for 6 d. As a positive control, macrophages were treated with 100 ng/mL LPS for 24 h. Cytokine production was quantified by ELISA. **e**,**f**). Macrophages were polarised to an M1 phenotype with IFNγ (10 ng/mL) for 24 h in the presence and absence of scaffolds. The mRNA expression was quantified by real-time PCR. (**b**) $p < 0.001$ and (**a**) $p < 0.05$.

Results

Porous scaffolds can be fabricated using porcine Growth Plate (GP) ECM

Scaffolds were generated by lyophilisation of slurries of GP matrix, resulting in constructs with an open, interconnected porosity, with a mean pore size of 126 ± 52 μm, suitable for cellular infiltration and migration (Fig. 1**a**). Biochemical analysis of decellularised GP (0.1 % SDS treatment) indicated that sGAG and calcium could be retained within the matrix, with no significant reduction in the levels of these ECM components compared to the untreated native GP control (Fig. 1**b**). A significant reduction in DNA content was observed following decellularisation.

The scaffolds were next assessed by culturing primary human macrophages in the presence of native and decellularised (0.1 % SDS) GP. LPS, a potent driver of pro-inflammatory cytokine production, was included as a positive control. No increase in IL-12 or TNF production was detected with either material (Fig. 2**a**,**b**). Robust IL-8 production was observed in the supernatants of macrophages cultured with native GP; however this was significantly lower with decellularised GP (Fig. 2**c**). Native GP produced comparable levels of IL-1β to LPS and again this was reduced in the presence of the decellularised material (Fig. 2**d**).

The effect of the scaffolds on M1-associated macrophage polarisation was next assessed. In this case, macrophages were cultured in the presence of native and decellularised GP prior to treatment with the M1 polarising cytokine, IFNγ. As expected, IFNγ increased the expression of the M1 associated genes, CCL19 and CXCL11, and this was not altered by the presence of the scaffolds (Fig. 2**e**,**f**).

MSC seeded GP ECM scaffolds mineralise in either chondrogenic or osteogenic culture conditions

Independent of the culture conditions, bone marrow derived MSCs cultured on GP scaffolds were observed to deposit a densely calcified matrix over 28 d *in vitro* (Fig. 3**a**,**b**). The constructs cultured in chondrogenic conditions stained

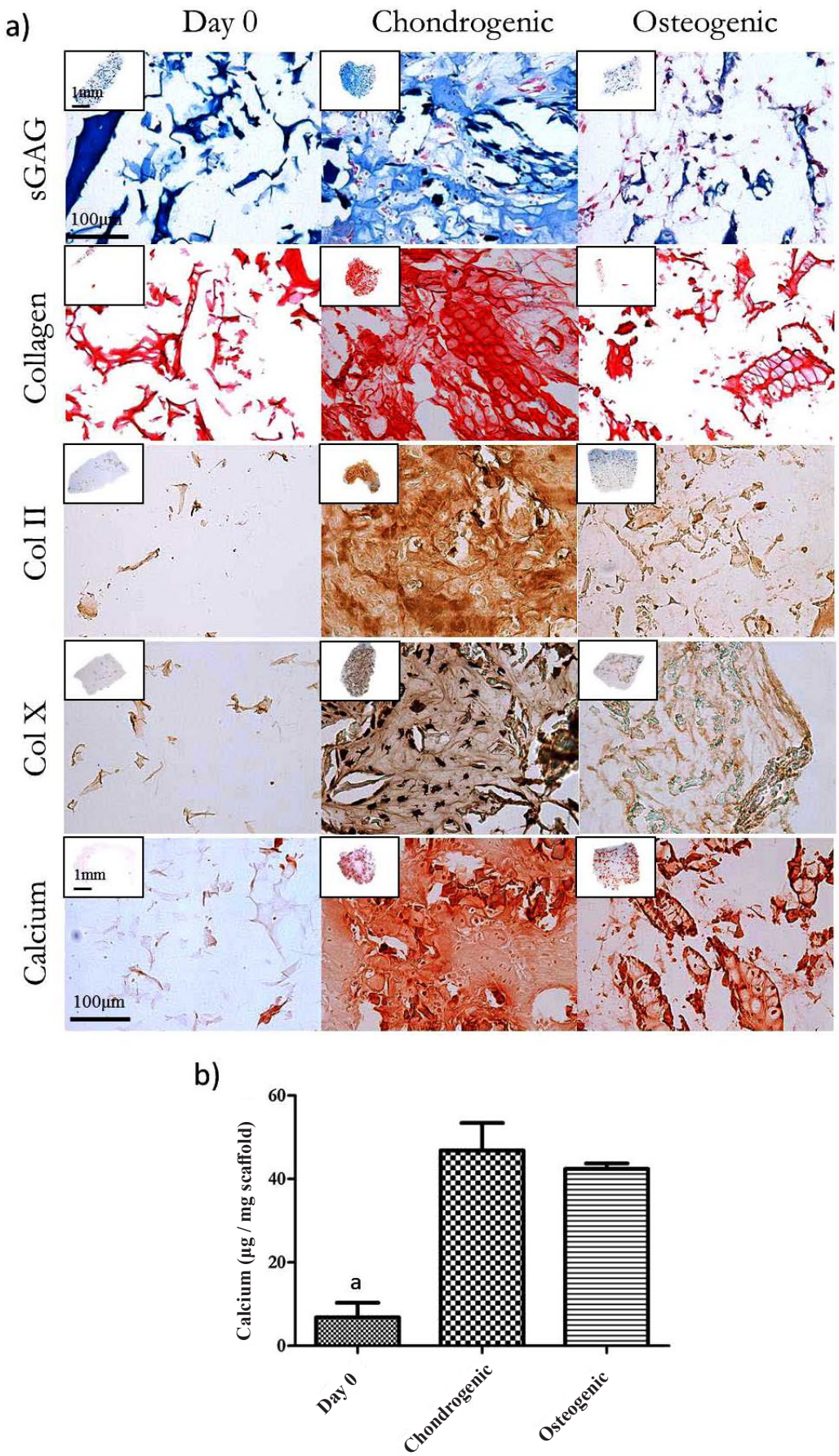


Fig. 3. **a**). Histological analysis of scaffolds at day 0, and MSC-seeded constructs after 28 d in either chondrogenic or osteogenic conditions. Deposition of sGAG, collagen, collagen type II and X and calcium is observed, particularly in the construct cultured in chondrogenic medium. **b**). Biochemical analysis of the calcium deposited by MSCs over the culture period (a) $p < 0.05$.

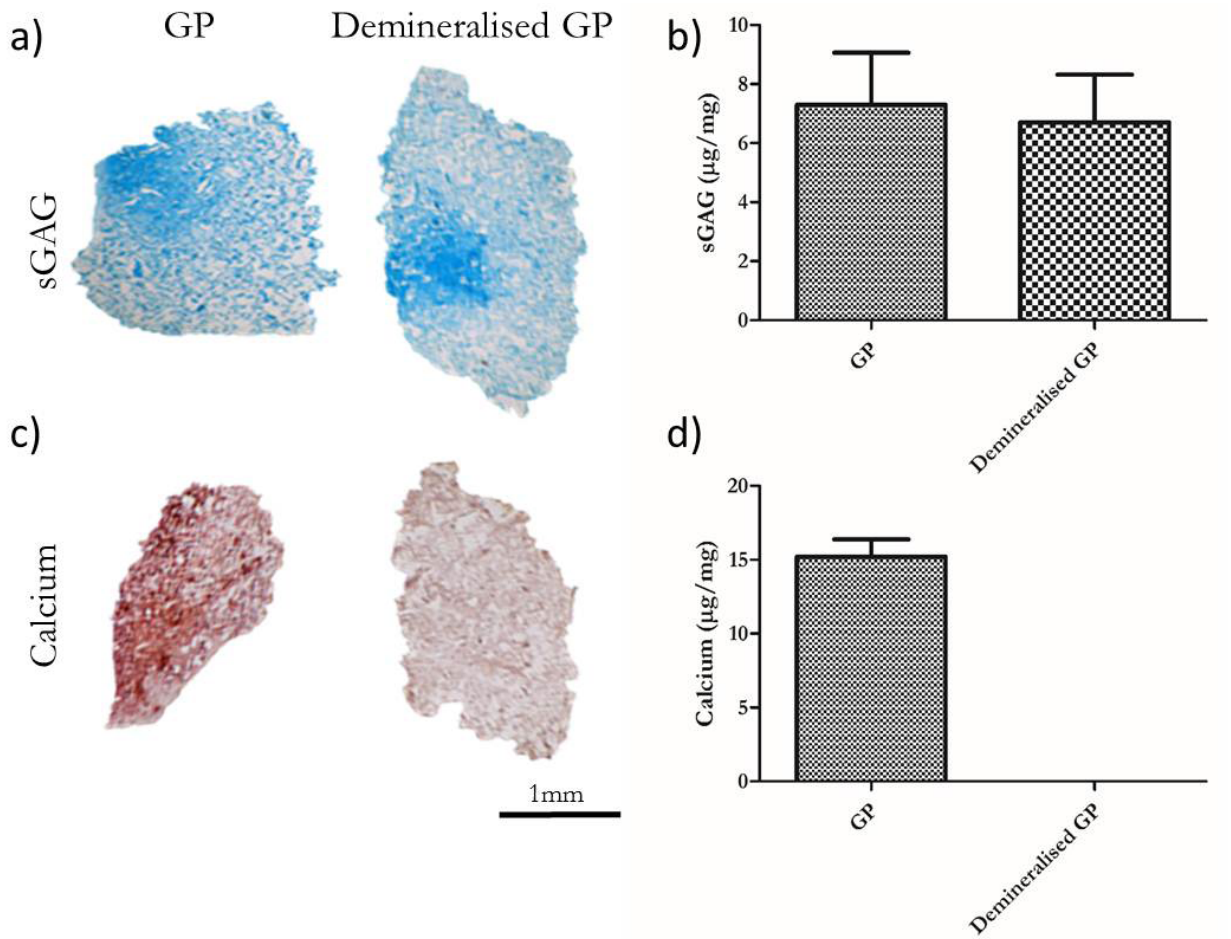


Fig. 4. **a**,**b**). Histological and biochemical analysis of sGAG deposition by MSCs at day 28 in chondrogenic culture conditions, seeded on a GP scaffold and a demineralised GP scaffold. **c**,**d**). Histological and biochemical analysis of calcium deposition occurring over the culture period on the GP and demineralised GP scaffolds.

more intensely for sGAG, collagen type II and type X after 28 d in culture compared to MSC-laden scaffolds cultured in osteogenic conditions, suggesting the development of a hypertrophic cartilage matrix that was calcifying *in vitro*. Quantification of the mineral deposition demonstrated that similar levels of calcium had accumulated within the scaffolds maintained in chondrogenic and osteogenic culture conditions (Fig. 3**b**).

In an attempt to elucidate the relative role of the unique collagenous matrix of the GP over other non-collagenous components in driving this cell-mediated mineral deposition, day 0 GP scaffolds were treated with EDTA in order to completely remove the mineral content prior to cell-seeding, leaving behind only a collagenous matrix (Day 0 calcium levels pre-decalcifying were 7.8 ± 0.3 µg/mg scaffold, and these values were subtracted from the day 28 results). Demineralised GP scaffolds were capable of supporting similar levels of sGAG accumulation over the 28 d in chondrogenic culture conditions; however, the ability of these scaffolds to induce mineralisation was significantly hampered (Fig. 4**a-d**), with no evidence of cell-mediated mineralisation detected in these constructs.

GP ECM derived scaffolds can accelerate endogenous bone regeneration in a critically-sized cranial defect

Having demonstrated the osteogenicity of GP ECM scaffolds *in vitro*, we next implanted them cell-free into 7 mm cranial defects, with healing analysed 4 and 8 weeks after implantation and compared to untreated controls. Reconstructed 3D µCT images demonstrated the widespread deposition of bone at both time points post-implant (Fig. 5**a**,**b**). Upon closer inspection, small nodules of mineral were found homogeneously distributed throughout the defect. Quantification of the bone volume per total defect volume (BV/TV) demonstrated significantly greater levels of mineralised tissue at both 4 and 8 weeks *vs.* empty groups (Fig. 5**c**).

Histological analysis (H&E) of the harvested samples demonstrated bone formation within the GP scaffold treated groups at 4 and 8 weeks, compared to predominantly fibrous tissue bridging the defect in the untreated group (Fig. 6**a**). Positive safranin-O staining for sGAG deposition was observed within the scaffold treated groups at 4 weeks, and to a lesser degree at 8 weeks (Fig. 6**b**). This appeared to be staining of the residual GP cartilage within the scaffold,

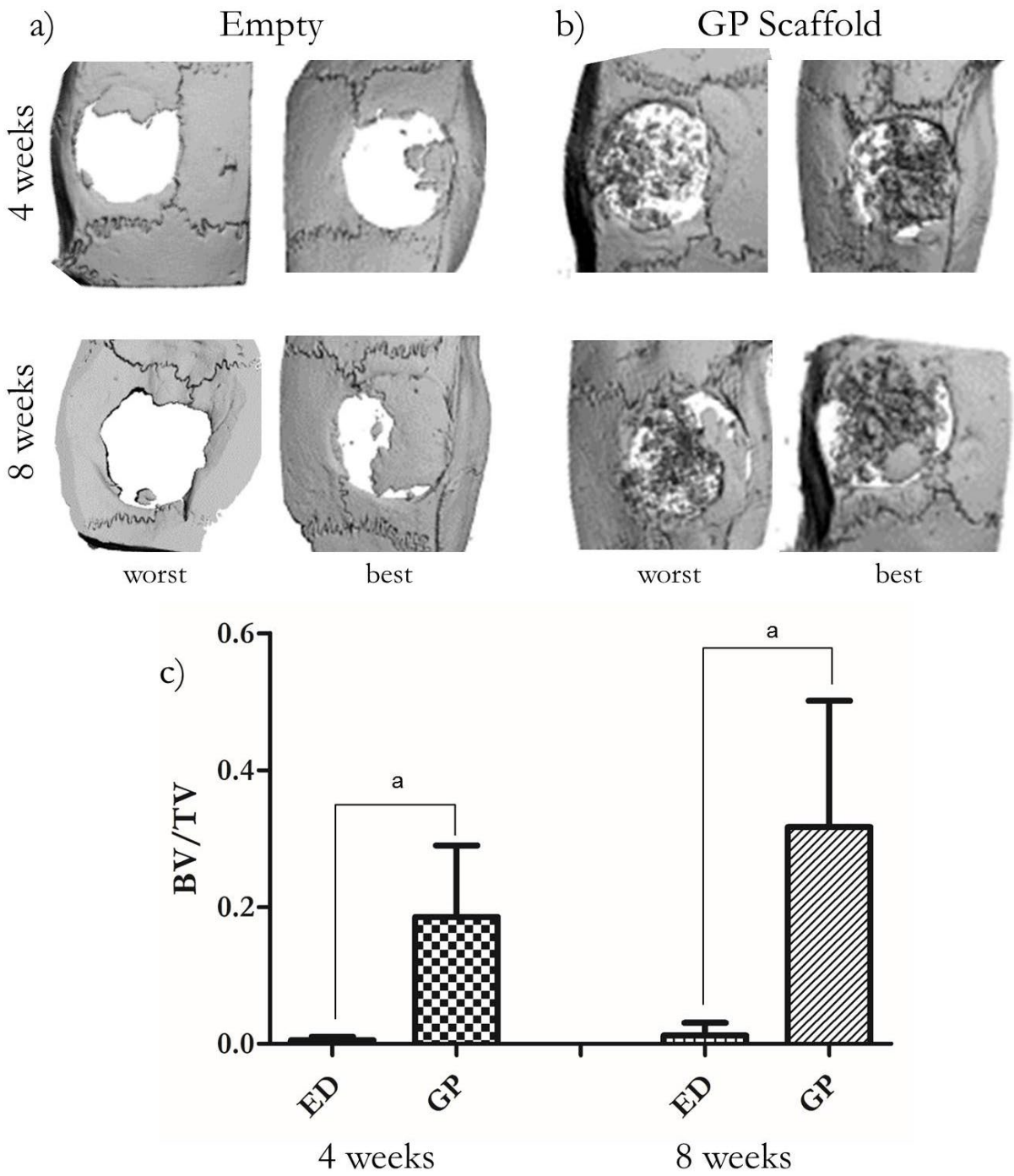


Fig. 5. **a**,**b**). Reconstructed µCT images indicate a distribution of mineral throughout GP scaffold treated defects, in comparison to the empty controls. **c**). A graph of the bone volume to total volume at both 4 and 8 weeks for GP treated and untreated (ED) groups. (**a**) $p < 0.05$.

and not evidence of bone forming *via* endochondral ossification. In addition, histomorphometric analysis of H&E stained slices allowed for determination of bone area within the defect, revealing a significant difference between the GP scaffold group and the empty control (Fig. 6**c**). Quantification of vessel number also indicated a significantly higher number of vessels were observed within the GP treated groups at both 4 and 8 weeks (Fig. 6**d**).

Discussion

The overall goal of this study was to develop porous scaffolds from GP ECM and to evaluate its potential as a biomaterial for promoting bone regeneration. The innate immune response of the scaffolds was assessed by culturing with primary human macrophages, which demonstrated that decellularisation resulted in reduced IL-1β and IL-8 production. These decellularised scaffolds were able to support osteogenesis of MSCs *in vitro* in both osteogenic

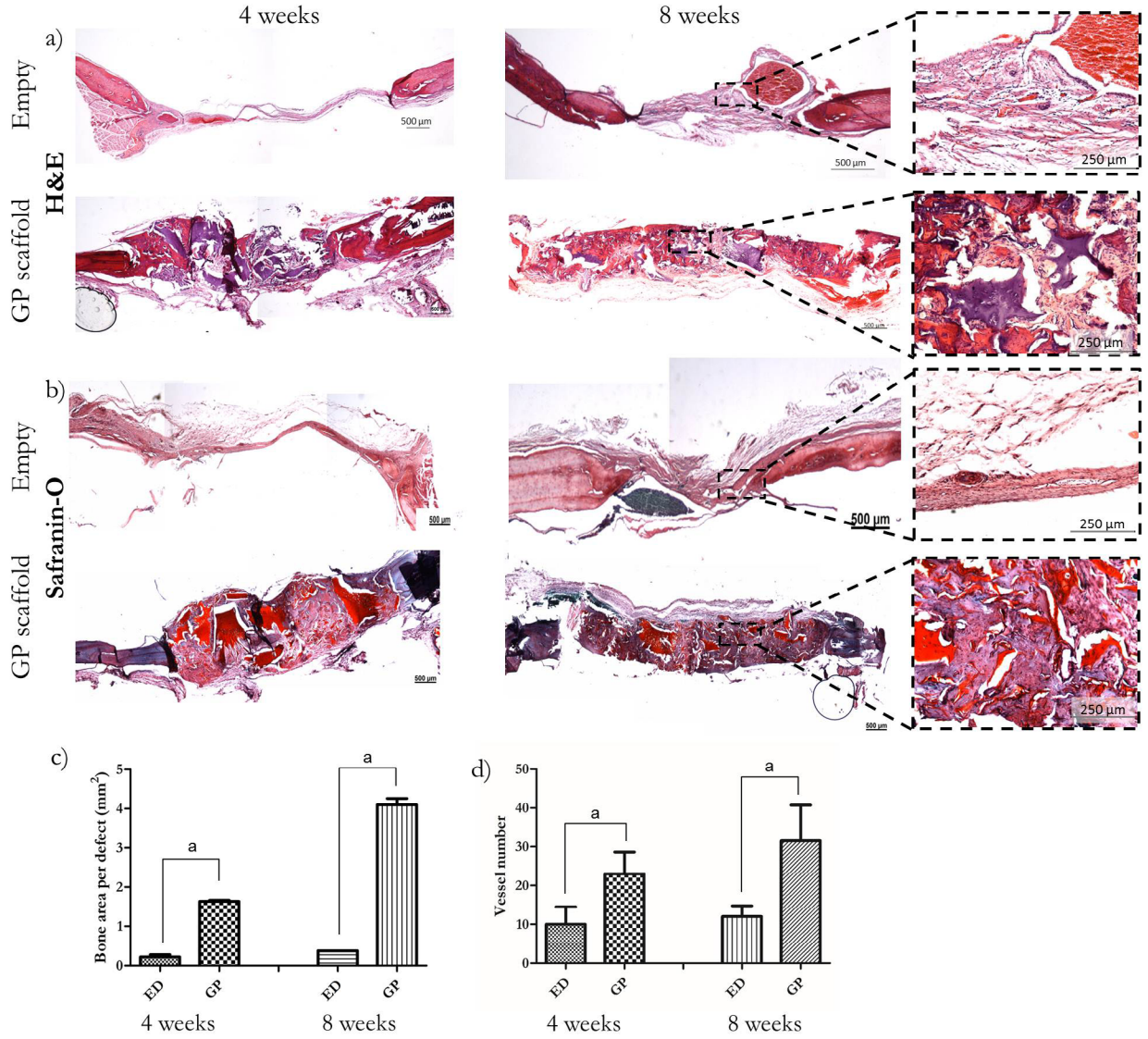


Fig. 6. **a-b**). Histological analysis of GP scaffold treated and empty cranial defects at 4 and 8 weeks post implantation, indicating *de novo* bone formation, sGAG, and collagen/connective tissue deposition. Higher magnification images are presented for the 8 week images. **c**,**d**). Quantification of the bone area per defect and vessel number within the defect at both time points (ED; empty defect, GP; growth plate). (**a**) $p < 0.05$.

and chondrogenic culture conditions, and their acellular implantation into a critically-sized defect accelerated vascularisation and endogenous bone formation and repair. Taken together, these findings indicate the potential of this novel ECM derived biomaterial for large bone defect healing.

Calcified tissue was observed in MSC-seeded GP scaffolds cultured in both chondrogenic and osteogenic conditions after 28 d *in vitro*. The presence of collagen type II, type X and sGAG indicate that the mineralisation achieved in chondrogenic media was occurring *via* an endochondral route compared to that arising in the constructs cultured in osteogenic media. GP scaffolds seeded with MSCs and cultured in standard expansion medium (containing serum) also extensively mineralised (data not shown). Interestingly, however, when the GP scaffold was further treated with a decalcifying agent prior to cell seeding, the matrix failed to induce any cell-mediated mineral deposition when maintained in chondrogenic culture conditions. This would suggest that the relatively low mineral component within the GP is a dominant osteoinductive component rather than the collagenous matrix itself, although at this stage we cannot rule out a potential role for other non-collagenous proteins and growth factors that may be removed by EDTA treatment. Further proteomic analysis of the GP post scaffold fabrication is required to fully identify the key matrix components influencing cell differentiation and bone formation.

Successful integration of ECM scaffolds is dependent on appropriate host immune responses; therefore, preliminary assays were carried out to examine their effect on primary human macrophages. The production of key pro-inflammatory cytokines and chemokines was assessed and, as demonstrated, the production of IL-12, which links innate and adaptive immune responses was minimal. This was also the case for the highly inflammatory cytokine, TNFα. Interestingly, native GP induced high

levels of the chemokine, IL-8, which is a key driver of neutrophil chemotaxis and has the potential to exacerbate inflammatory responses. Importantly, decellularisation of GP with 0.1 % SDS reduced IL-8 production by approximately 50 %. It will be interesting to determine the precise role played by this chemokine in host interactions with ECM scaffolds. Of note, it has been shown that IL-8 can promote osteoclastogenesis (Kopesky *et al.*, 2014); therefore, a certain level of this protein may actually be beneficial for optimal remodelling. We also assessed the effect of the scaffolds on macrophage phenotype given that they are likely to be implanted into an inflammatory micro-environment. Encouragingly, the scaffolds did not enhance the expression of genes that are associated with an inflammatory M1 macrophage phenotype. Furthermore, treatment with SDS appeared to reduce the expression of some M1 associated markers.

The only evidence of native GP material being used to treat bone defects, to the best of our knowledge, was in a series of recent studies where GP tissue was demineralised in a manner similar to bone matrix (DBM), and the resultant powder used to fill bone defects. This demineralised GP powder demonstrated an ability to achieve mineralisation *in vivo,* both ectopically in rat muscle, and orthopically in a rat spine defect and a rabbit radial defect study (Bigham-Sadegh *et al.*, 2014; Bigham *et al.*, 2011; Shadkhast and Bighamsadegh, 2011). These studies pointed to the presence of potent growth factors from the TGF-β super-family within the GP matrix as potentially leading to the observed bone deposition. In a similar study, the authors reported enhanced bone formation when the demineralised GP powder was supplemented with synthetic hydroxyapatite (Bigham-Sadegh *et al.*, 2015). This may be related to the *in vitro* results observed in this study, where EDTA treatment to remove the calcium within the GP scaffolds was found to dramatically reduce their capacity to support an endochondral phenotype.

Analysis of defects treated with an acellular GP scaffold illustrated that endogenous cells were capable of infiltrating throughout the porous scaffold, facilitating mineralisation and *de novo* bone formation by 4 weeks. Quantification of the bone volume also indicates the beneficial effect of implanting the GP scaffold, with enhanced levels observed by 4 weeks. This distribution throughout the implanted material is highly favourable, as constructs can often become surrounded by new tissue, with mineralisation observed predominantly on the periphery of the implanted material, leading to core necrosis and implant failure (Lyons *et al.*, 2010). The high porosity of the scaffold clearly facilitated excellent cell infiltration and vessel in-growth, which ultimately contributed to the enhanced bone formation observed throughout the defect. The GP matrix is known to contain potent angiogenic growth factors which may have played a role in enhancing angiogenesis within the scaffold treated defects (Qiu *et al.*, 2015). Comparable studies in the literature, using collagen based scaffolds to treat rat cranial defects, have demonstrated the need to incorporate exogenous factors such as BMP-2 (Quinlan *et al.*, 2015b) and/or VEGF (Curtin *et al.*, 2014) to induce robust bone healing. The fact that GP derived scaffolds can promote healing without the need for the additional delivery of exogenous factors such as BMP-2, which can have potent off-target effects (Benglis *et al.*, 2008; Cahill *et al.*, 2009), points to their potential use as a safe, low-cost and effective biomaterial for the repair or large bone defects. It should be noted, however, that our studies have been performed in relatively low-load bearing defects, and follow-up studies are required to assess their efficacy in more mechanically challenging locations.

While positive staining for cartilage specific matrix components was observed in scaffold treated defects, this was predominately staining of residual scaffold material and not necessarily evidence of endochondral bone healing, although we cannot completely rule out the possibility of this occurring. Cranial bones form *via* intramembranous ossification during embryonic development, although previous studies have also shown that healing in this region can occur along the endochondral route (Jukes *et al.*, 2008; Lin *et al.*, 2013). Future studies are required to further quantify the exact temporal patterns of repair within defects treated with GP ECM derived scaffolds.

Analysing the quality of the *de novo* tissue forming in more detail showed that newly deposited bone was replacing the GP ECM scaffold, with remodelling of the scaffold evident between week 4 and 8, as demonstrated by a reduction in residual scaffold material within the defect over time. However, it should be noted that there was some variability observed within scaffolds, due to the different sizes of GP particles used to form the 3D scaffolds. This limitation can be avoided in future studies through the use of a cryo-mill which can generate a more homogeneous GP particle size range, which would lead to less variation from batch to batch (Almeida *et al.*, 2015). In addition, more stringent decellularisation protocols will be developed, which will be particularly important when translating this scaffold material towards clinical applications (Badylak, 2004); however, no evidence of a chronic immune response was detected at either time point in the scaffold treated groups.

Conclusions

This study provides data to support the use of scaffolds derived from decellularised growth plate ECM for the repair of critically-sized bone defects. MSCs seeded on the GP scaffold *in vitro* underwent robust osteogenesis in both chondrogenic and osteogenic culture conditions. Upon implantation within a critically-sized cranial defect, the acellular GP scaffold facilitated endogenous cell infiltration and the deposition of a mineralised *de novo* bone matrix, with significantly more blood vessels and higher levels of bone formation compared to the empty controls, illustrating the potential of GP ECM as a biomaterial for bone regeneration. These scaffolds are relatively easy to produce in a process that could be readily scaled up. The fact that these scaffolds promote enhanced bone healing without the requirement for functionalisation with endogenous factors such as BMP-2 points to their potential as a safe and cost-effective biomaterial for treating large bone defects.

Acknowledgements

Funding for this work was provided by AO under the large bone defect healing program, Science Foundation Ireland (12/IA/1554) in addition to the Health Research Board of Ireland (Grant No. HRA_POR/2011/27) and the European Research Council (ERC Grant Agreement No. 239685).

References

Aghdasi B, Montgomery SR, Daubs MD, Wang JC (2013) A review of demineralized bone matrices for spinal fusion: the evidence for efficacy. Surgeon **11**: 39-48.

Alini M, Matsui Y, Dodge G, Poole AR (1992) The extracellular matrix of cartilage in the growth plate before and during calcification: Changes in composition and degradation of type II collagen. Calcif Tissue Int **50**: 327-335.

Almeida HV, Cunniffe GM, Vinardell T, Buckley CT, O'Brien FJ, Kelly DJ (2015) Coupling freshly isolated CD44(+) infrapatellar fat pad-derived stromal cells with a TGF-beta3 eluting cartilage ECM-derived scaffold as a single-stage strategy for promoting chondrogenesis. Adv Healthc Mater **4**: 1043-1053.

Almeida HV, Liu Y, Cunniffe GM, Mulhall KJ, Matsiko A, Buckley CT, O'Brien FJ, Kelly DJ (2014) Controlled release of transforming growth factor-β3 from cartilage-extra-cellular-matrix-derived scaffolds to promote chondrogenesis of human-joint-tissue-derived stem cells. Acta Biomater **10**: 4400-4409.

An HS, Simpson JM, Glover JM, Stephany J (1995) Comparison between allograft plus demineralized bone matrix *versus* autograft in anterior cervical fusion: a prospective multicenter study. Spine **20**: 2211-2216.

Anderson HC, Hodges PT, Aguilera XM, Missana L, Moylan PE (2000) Bone morphogenetic protein (BMP) localization in developing human and rat growth plate, metaphysis, epiphysis, and articular cartilage. J Histochem Cytochem **48**: 1493-1502.

Badylak SF (2004) Xenogeneic extracellular matrix as a scaffold for tissue reconstruction. Transpl Immunol **12**: 367-377.

Benders KEM, Weeren PRv, Badylak SF, Saris DBF, Dhert WJA, Malda J (2013) Extracellular matrix scaffolds for cartilage and bone regeneration. Trends Biotechnol **31**: 169-176.

Benglis D, Wang MY, Levi AD (2008) A comprehensive review of the safety profile of bone morphogenetic protein in spine surgery. Neurosurgery **62**: 423-431.

Bigham-Sadegh A, Karimi I, Oryan A, Mahmoudi E, Shafiei-Sarvestani Z (2014) Spinal fusion with demineralized calf fetal growth plate as novel biomaterial in rat model: a preliminary study. Int J Spine Surg **8**: doi: 10.14444/1005.

Bigham-Sadegh A, Karimi I, Shadkhast M, Mahdavi MH (2015) Hydroxyapatite and demineralized calf fetal growth plate effects on bone healing in rabbit model. J Orthop Traumatol **16**: 141-149.

Bigham AS, Shadkhast M, Bigham Sadegh A, Shafiei Z, Lakzian A, Khalegi MR (2011) Evaluation of osteoinduction properties of the demineralized bovine foetal growth plate powder as a new xenogenic biomaterial in rat. Res Vet Sci **91**: 306-310.

Cahill KS, Chi JH, Day A, Claus EB (2009) Prevalence, complications, and hospital charges associated with use of bone-morphogenetic proteins in spinal fusion procedures. JAMA **302**: 58-66.

Calabrese G, Giuffrida R, Fabbi C, Figallo E, Lo Furno D, Gulino R, Colarossi C, Fullone F, Giuffrida R, Parenti R, Memeo L, Forte S (2016) Collagen-hydroxyapatite scaffolds induce human adipose derived stem cells osteogenic differentiation *in vitro*. PLoS one **11**: e0151181. doi: 10.1371/journal.pone.0151181.

Carlevaro MF, Cermelli S, Cancedda R, Descalzi Cancedda F (2000) Vascular endothelial growth factor (VEGF) in cartilage neovascularization and chondrocyte differentiation: auto-paracrine role during endochondral bone formation. J Cell Sci **113**: 59-69.

Chen G, Lv Y, Dong C, Yang L (2015) Effect of internal structure of collagen/hydroxyapatite scaffold on the osteogenic differentiation of mesenchymal stem cells. Curr Stem Cell Res Ther **10**: 99-108.

Cheng CW, Solorio LD, Alsberg E (2014) Decellularized tissue and cell-derived extracellular matrices as scaffolds for orthopaedic tissue engineering. Biotechnol Adv **32**: 462-484.

Corr EM, Cunningham CC, Dunne A (2016) Cholesterol crystals activate Syk and PI3 kinase in human macrophages and dendritic cells. Atherosclerosis **251**: 197-205.

Cunniffe GM, Curtin CM, Thompson EM, Dickson GR, O'Brien FJ (2016) Content-dependent osteogenic response of nanohydroxyapatite: an *in vitro* and *in vivo* assessment within collagen-based scaffolds. ACS Appl Mater Interfaces **8**: 23477-23488.

Cunniffe GM, Dickson GR, Partap S, Stanton KT, O'Brien FJ (2010) Development and characterisation of a collagen nano-hydroxyapatite composite scaffold for bone tissue engineering. J Mater Sci Mater Med **21**: 2293-2298.

Cunniffe GM, O'Brien FJ (2011) Collagen scaffolds for orthopedic regenerative medicine. JOM **63**: 66-73.

Cunniffe GM, Vinardell T, Murphy JM, Thompson EM, Matsiko A, O'Brien FJ, Kelly DJ (2015) Porous decellularized tissue engineered hypertrophic cartilage as a scaffold for large bone defect healing. Acta Biomater **23**: 82-90.

Curtin CM, Tierney EG, McSorley K, Cryan SA, Duffy GP, O'Brien FJ (2014) Combinatorial gene therapy accelerates bone regeneration: non-viral dual delivery of VEGF and BMP2 in a collagen-nanohydroxyapatite scaffold. Adv Healthc Mater **4**: 223-227.

David F, Levingstone TJ, Schneeweiss W, de Swarte M, Jahns H, Gleeson JP, O'Brien FJ (2015) Enhanced bone healing using collagen-hydroxyapatite scaffold implantation in the treatment of a large multiloculated mandibular aneurysmal bone cyst in a thoroughbred filly. J Tissue Eng Regen Med **9**: 1193-1199.

Dimitriou R, Jones E, McGonagle D, Giannoudis PV (2011) Bone regeneration: current concepts and future directions. BMC Med **9**: 66. doi: 10.1186/1741-7015-9-66.

Gerber HP, Vu TH, Ryan AM, Kowalski J, Werb Z, Ferrara N (1999) VEGF couples hypertrophic cartilage

remodeling, ossification and angiogenesis during endochondral bone formation. Nat Med **5**: 623-628.

Gilbert TW, Sellaro TL, Badylak SF (2006) Decellularization of tissues and organs. Biomaterials **27**: 3675-3683.

Gleeson JP, Plunkett NA, O'Brien FJ (2010) Addition of hydroxyapatite improves stiffness, interconnectivity and osteogenic potential of a highly porous collagen-based scaffold for bone tissue regeneration. Eur Cell Mater **20**: 218-230.

Gruskin E, Doll BA, Futrell FW, Schmitz JP, Hollinger JO (2012) Demineralized bone matrix in bone repair: History and use. Adv Drug Deliv Rev **64**: 1063-1077.

Haugh MG, Jaasma MJ, O'Brien FJ (2009) The effect of dehydrothermal treatment on the mechanical and structural properties of collagen-GAG scaffolds. J Biomed Mater Res A **89**: 363-369.

Jin CZ, Park SR, Choi BH, Park K, Min B-H (2007) *In vivo* cartilage tissue engineering using a cell-derived extracellular matrix scaffold. Artif Organs **31**: 183-192.

Jukes JM, Both SK, Leusink A, Sterk LMT, Van Blitterswijk CA, De Boer J (2008) Endochondral bone tissue engineering using embryonic stem cells. Proc Natl Acad Sci U S A **105**: 6840-6845.

Karageorgiou V, Kaplan D (2005) Porosity of 3D biomaterial scaffolds and osteogenesis. Biomaterials **26**: 5474-5491.

Kheir E, Stapleton T, Shaw D, Jin Z, Fisher J, Ingham E (2011) Development and characterization of an acellular porcine cartilage bone matrix for use in tissue engineering. J Biomed Mater Res A **99**: 283-294.

Kim IG, Hwang MP, Du P, Ko J, Ha C-w, Do SH, Park K (2015) Bioactive cell-derived matrices combined with polymer mesh scaffold for osteogenesis and bone healing. Biomaterials **50**: 75-86.

Kopesky P, Tiedemann K, Alkekhia D, Zechner C, Millard B, Schoeberl B, Komarova SV (2014) Autocrine signaling is a key regulatory element during osteoclastogenesis. Biol Open **3**: 767-776.

Kronenberg HM (2003) Developmental regulation of the growth plate. Nature **423**: 332-336.

Lau TT, Lee LQP, Vo BN, Su K, Wang D-A (2012) Inducing ossification in an engineered 3D scaffold-free living cartilage template. Biomaterials **33**: 8406-8417.

Lin C-Y, Chang Y-H, Li K-C, Lu C-H, Sung L-Y, Yeh C-L, Lin K-J, Huang S-F, Yen T-C, Hu Y-C (2013) The use of ASCs engineered to express BMP2 or TGF-β3 within scaffold constructs to promote calvarial bone repair. Biomaterials **34**: 9401-9412.

Lu H, Hoshiba T, Kawazoe N, Chen G (2011) Autologous extracellular matrix scaffolds for tissue engineering. Biomaterials **32**: 2489-2499.

Luo L, Chu JYJ, Eswaramoorthy R, Mulhall KJ, Kelly DJ (2016) Engineering tissues that mimic the zonal nature of articular cartilage using decellularized cartilage explants seeded with adult stem cells. ACS Biomater. Sci. Eng. doi: 10.1021/acsbiomaterials.6b00020

Luo L, Eswaramoorthy R, Mulhall KJ, Kelly DJ (2015) Decellularization of porcine articular cartilage explants and their subsequent repopulation with human chondroprogenitor cells. J Mech Behav Biomed Mater **55**: 21-31.

Lyons FG, Al-Munajjed AA, Kieran SM, Toner ME, Murphy CM, Duffy GP, O'Brien FJ (2010) The healing of bony defects by cell-free collagen-based scaffolds compared to stem cell-seeded tissue engineered constructs. Biomaterials **31**: 9232-9243.

Murphy CM, Haugh MG, O'Brien FJ (2010) The effect of mean pore size on cell attachment, proliferation and migration in collagen-glycosaminoglycan scaffolds for bone tissue engineering. Biomaterials **31**: 461-466.

Nilsson O, Parker EA, Hegde A, Chau M, Barnes KM, Baron J (2007) Gradients in bone morphogenetic protein-related gene expression across the growth plate. J Endocrinol **193**: 75-84.

O'Brien FJ, Harley BA, Waller MA, Yannas IV, Gibson LJ, Prendergast PJ (2007) The effect of pore size on permeability and cell attachment in collagen scaffolds for tissue engineering. Technol Health Care **15**: 3-17.

Pati F, Song TH, Rijal G, Jang J, Kim SW, Cho DW (2015) Ornamenting 3D printed scaffolds with cell-laid extracellular matrix for bone tissue regeneration. Biomaterials **37**: 230-241.

Pattabhi SR, Martinez JS, Keller Iii TCS (2014) Decellularized ECM effects on human mesenchymal stem cell stemness and differentiation. Differentiation **88**: 131-143.

Prosecka E, Rampichova M, Litvinec A, Tonar Z, Kralickova M, Vojtova L, Kochova P, Plencner M, Buzgo M, Mickova A, Jancar J, Amler E (2015) Collagen/hydroxyapatite scaffold enriched with polycaprolactone nanofibers, thrombocyte-rich solution and mesenchymal stem cells promotes regeneration in large bone defect *in vivo*. J Biomed Mater Res A **103**: 671-682.

Qiu T, Xian L, Crane J, Wen C, Hilton M, Lu W, Newman P, Cao X (2015) PTH receptor signaling in osteoblasts regulates endochondral vascularization in maintenance of postnatal growth plate. J Bone Miner Res **30**: 309-317.

Quinlan E, Lopez-Noriega A, Thompson EM, Hibbitts A, Cryan SA, O'Brien FJ (2015a) Controlled release of vascular endothelial growth factor from spray-dried alginate microparticles in collagen-hydroxyapatite scaffolds for promoting vascularization and bone repair. J Tissue Eng Regen Med. doi: 10.1002/term.2013.

Quinlan E, Thompson EM, Matsiko A, O'Brien FJ, Lopez-Noriega A (2015b) Long-term controlled delivery of rhBMP-2 from collagen-hydroxyapatite scaffolds for superior bone tissue regeneration. J Control Release **207**: 112-119.

Safi W, Kuehnl A, Nüssler A, Eckstein H-H, Pelisek J (2016) Differentiation of human CD14+ monocytes: an experimental investigation of the optimal culture medium and evidence of a lack of differentiation along the endothelial line. Exp Mol Med **48**: e227. doi: 10.1038/emm.2016.11.

Samorezov JE, Alsberg E (2015) Spatial regulation of controlled bioactive factor delivery for bone tissue engineering. Adv Drug Deliv Rev **84**: 45-67.

Shadkhast M, Bighamsadegh A (2011) Demineralized calf foetal growth plate effects on experimental bone healing. Bone **48**: S168.

Sheehy EJ, Mesallati T, Kelly L, Vinardell T, Buckley CT, Kelly DJ (2015) Tissue engineering whole bones through endochondral ossification: regenerating the distal phalanx. Biores Open Access **4**: 229-241.

Solheim E (1998) Growth factors in bone. Int Orthop **22**: 410-416.

Sutherland AJ, Converse GL, Hopkins RA, Detamore MS (2015) The bioactivity of cartilage extracellular matrix in articular cartilage regeneration. Adv Healthc Mater **4**: 29-39.

Tilkeridis K, Touzopoulos P, Ververidis A, Christodoulou S, Kazakos K, Drosos GI (2014) Use of demineralized bone matrix in spinal fusion. World J Orthop **5**: 30-37.

Villa MM, Wang L, Huang J, Rowe DW, Wei M (2015) Bone tissue engineering with a collagen-hydroxyapatite scaffold and culture expanded bone marrow stromal cells. J Biomed Mater Res B Appl Biomater **103**: 243-253.

Wang Y, Middleton F, Horton JA, Reichel L, Farnum CE, Damron TA (2004) Microarray analysis of proliferative and hypertrophic growth plate zones identifies differentiation markers and signal pathways. Bone **35**: 1273-1293.

Discussion with reviewers

Reviewer 1: Do the authors have an idea which non collagneous ECM proteins would be removed by EDTA and which would be likely to remain in the demineralised scaffold?

Authors: EDTA treatment step is a commonly used de-calcifying agent, although its complete effects are not easy to evaluate. It has been demonstrated that EDTA removes calcium phosphate, bone sialoprotein and decorin from bone tissue (Gerstenfeld *et al*., 1994), while others indicate that it removes phosphoproteins from teeth in addition to calcium and diffusible phosphate (Dimuzio and Veis, 1978). We have not studied the specific components that are being removed from the growth plate tissue, and hope to accomplish this in the future with in depth proteomic analysis. We believe that the major component removed is the mineral phase, but wanted to account for the fact that other non-collagenous proteins may also be removed during EDTA treatment.

In our osteogenic culture conditions, all scaffolds tend to support robust cell differentiation down an osteogenic pathway, with high levels of mineral deposition achieved by day 28. Subtle differences are not easily observed using these potent osteogenic culture conditions, and as such, were not included within this section.

The EDTA treated scaffold "Demineralised GP" stained positively for collagen (Fig. 7); however, we did not do immunohistochemistry for specific Col X presence. We believe the collagens present to be similar to those observed in the non-EDTA treated GP scaffolds, namely Col II and Col X.

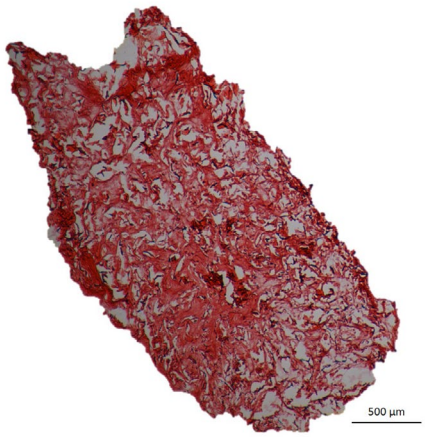


Fig. 7. Demineralised GP scaffold treated with EDTA and cultured in chondrogenic culture conditions for 28 d stained positively for collagen using picrosirius red staining.

Reviewer II: The use of rat calvaria defects are commonplace for testing bone constructs. However, they do not test the effect of mechanical loading on bone healing and remodelling. Could the authors discuss their decision to use this model with reference to the three Rs?

Authors: Porous scaffold materials such as the ECM scaffold, presented in this publication, would be suitable for non-load bearing maxillofacial applications, or would require the use of a fixation device within a load-bearing site. The rat calvarial defect model is widely used for testing bone regeneration strategies due to its versatility and reproducibility. In our hands, the model also has the benefit of minimal morbidity and periprocedural mortality rates. They are deemed appropriate analogues to the clinical condition they are used to investigate (Spicer *et al*., 2012).

Additional References

Dimuzio MT, Veis A (1978) The biosynthesis of phosphophoryns and dentin collagen in the continuously erupting rat incisor. J Biol Chem **253**: 6845-6852.

Gerstenfeld LC, Feng M, Gotoh Y, Glimcher MJ (1994) Selective extractability of noncollagenous proteins from chicken bone. Calcif Tissue Int **55**: 230-235.

Spicer PP, Kretlow JD, Young S, Jansen JA, Kasper FK, Mikos AG (2012) Evaluation of bone regeneration using the rat critical size calvarial defect. Nat Protoc **7**: 1918-1929.

Editor's note: The Scientific Editor responsible for this paper was Chris Evans